Accounting for pipeline thermal capacity in district heating simulations

Accounting for pipeline thermal capacity in district heating simulations

Martina Capone[a)], Elisa Guelpa[b)] and Vittorio Verda[c)]

Energy Department, Politecnico di Torino, Corso Duca Degli Abruzzi 24, 10129 Torino, Italy

[a)]Corresponding author: martina.capone@polito.it
[b)]elisa.guelpa@polito.it
[c)]vittorio.verda@polito.it

Abstract. The transition towards 4th generation systems is making district heating increasingly efficient and complex: a broad variety of novelties are being introduced, like the ever-growing integration of renewable sources, the use of lower operating temperatures, the interaction with other energy grids. These new elements are challenging the features of existing numerical models, which may be better analyzed and revisited taking into account the even more important role assumed by thermal transients. In this framework, the aim of this paper is to study the effect of the heat capacities of the steel pipe and of the insulation layer on the thermal response of the systems. Four different approaches are presented and compared: a one-equation model, a two-equations model, a three-equation model, and an equivalent one-equation model. These approaches are tested over a pure advection problem in a long pipe. The performances of each model are evaluated both in terms of accuracy and computational effort. Then, an application to the Turin district heating network, is discussed. Results show that the equivalent one-equation model is capable to produce accurate solutions with impressive computational time reductions (more than 96%) with respect to the more detailed methods.

Keywords: Network modelling; thermal behavior; heat capacity; equivalent model; thermal delay.

1. Introduction

District heating (DH) is a convenient solution to improve the energy efficiency of heating systems in communities [1]. Today it is recognized that this technology can have a key role in the cost-effective decarbonization of the European energy system [2]. Despite DH infrastructures are widely spread in Europe since the 1970s [3], nowadays these systems are experiencing a gradual transition towards a new generation, which is aimed at reaching a future non-fossil energy system based on completely renewable energy sources such as solar, waste heat and geothermal energy [4]. This have led to the conceptualization of 4th generation district heating (4GDH) [5,6], which is characterized by new features such as lower operating temperatures and lower grid losses, the possibility to recycle heat from low-temperature sources and integrate renewable heat sources and the ability to be part of an integrated smart energy system [5].

In this framework, it becomes essential to use suitable numerical models to simulate, design and optimize the configuration of existing and planned district heating networks. In the literature, multiple approaches have been developed for district heating modelling. They can be grouped in two major families: black-box models and physical models [7]. Black-box models are based on standard transfer function models or neural networks. These methods suffer from low accuracy in the time-delay estimation, especially when there are abrupt temperature changes [7]. On the other hand, physical models address the physical description of all the relevant components of a network. For this reason, they are preferred when large and quick temperature changes occur within the network and when the estimation of physical parameters is relevant [8]. Among the physical models, many different approaches can be found. The element method and the node method, introduced by Benonysson [9], have been used in many contributions [7,10].

Other popular methods are the characteristics method [11,12], the plug-flow model [13,14] and the finite volume method [8,12]. This last method will also be used in this paper.

Since the transition towards the fourth generation heavily affects the thermal dynamics within the network, having a tool which allows to accurately describe the thermal response of district heating systems is becoming more and more important. Thus, there is a need of defining which are the relevant parameters to take into account in a thermal model. Indeed, the aforementioned methods often uses many different approximations for some different aspects of the model. An example is the heat capacity of the pipe. The influence of this parameter is neglected by many authors in literature [12-13,19]. An example is the study proposed by Wang et al. [12], who uses a model that relies on a single partial differential equation including just the water thermal capacity to find the optimal scales of time and spatial steps for two different methods, namely implicit upwind model and characteristic line model. On the other hand, the pipe heat capacity is explicitly considered by other authors [10,15-18]. Among them, the function method introduced by Zheng et. al [15] is based on two balance equations – one for the pipe wall and one for the fluid. Moreover, Sartor and Dewalef [18] showed that the pipe thermal inertia produces a delay on the outlet pipe temperature response.
In this context, it becomes essential to compare the different formulations to understand whether it is worthy to increase the complexity of a district heating network model in order to include the thermal capacity of the pipe. Hence, , the aim of the current study is a) to analyze the influence of the heat capacity of the steel pipe (and alsoof the insulation layer) on the thermo-fluid dynamic behavior of a district heating network and b) to find an approach which allows to consider all the relevant parameters without jeopardizing the viability of the application with unreasonable CPU times. To do that. four different formulations of the thermal problem are compared. The first formulation involves a single partial differential equation which describes the thermal evolution of water and neglects the two contributions of the steel pipe heat capacity and of the insulation layer heat capacity. The second one is made up by two partial differential equations, taking into account the thermal evolution of water and steel. The third formulation contains all the contributions by means of a three-equation model. Finally, a fourth *equivalent* formulation combines the heat capacities of water and steel in a unique one-equation model, by approximating the two temperature evolutions as equal, while the heat capacity of insulation is again neglected.

The comparison of the four models is performed over a pure-advection model problem in a pipe. Finally, the performances of the standard one-equation model and of the equivalent one-equation model were tested on a real application. A case-study taken from the Turin district heating network, which is among the largest systems in Europe, is presented and discussed.

2. Methodology

In this section, the model used to simulate the thermo-fluid dynamic behavior of the district heating network is presented. The model aims at reproducing the evolution of pressures, mass-flow rates and temperatures within the whole system. Since different formulations are adopted for the thermal model, the differences among them are discussed and explained.

The model is based on a pseudo-dynamic approach: while the hydraulic problem, expressed by the conservation equations of mass and momentum, is treated as steady-state, the energy equation is solved dynamically. This is due to the fact that the fluid-dynamic perturbations are quickly transferred to the whole network, in a period of time of few seconds. In contrast, temperature perturbations travel at the fluid velocity and could take a long time to be propagated within the network.

The problem was treated as one-dimensional and the complex structure of the network was described by means of the graph theory [20]. Hence, each pipe was treated as a branch which connects two nodes, corresponding to the inlet and the outlet sections. The network topology was described by means of the incidence matrix **A**, which has as many rows as the number of nodes (*NN*) and as many columns as the number of branches (*NB*). The general element A_{ij} is equal to 1 if the i-th node is the inlet node of the j-th branch, -1 if the i-th node is the outlet node of the j-th branch and 0 if the i-th node and the j-th branch are not related to each other.

The finite volume method [21] was adopted for the solution of the problem. In particular, the continuity and energy equations were integrated over control volumes including each junction node and half of the branches entering or exiting that node. Actually, in the case of the energy equation, a greater number of control volumes was used in order to limit the effect of numerical diffusivity by reducing the mesh size [21]. Instead, the momentum equation was integrated over control volumes including a branch and the two delimiting nodes.

2.1 The hydraulic problem

The hydraulic problem can be expressed by the conservation equations of mass and momentum, respectively reported in Eq. (1) and Eq. (2):

$$\frac{\partial \rho_w}{\partial t} + \frac{\partial (\rho_w v_w)}{\partial x} = 0 \tag{1}$$

$$\rho_w \frac{\partial v_w}{\partial t} + \rho_w v_w \frac{\partial v_w}{\partial x} = -\frac{\partial p_w}{\partial x} - F_{FRICT} + F_1 \tag{2}$$

where F_{FRICT} takes into account the viscous forces and F_1 represents the source term accounting for the effect of local fluid dynamic resistance due to valves or junctions and the effects of pressure rise due to pumps. If steady-state conditions are considered, as previously explained, and continuity and momentum equations are integrated according to the finite volume method, the following formulation of the hydraulic problem can be obtained:

$$\mathbf{A} \cdot \mathbf{G} + \mathbf{G_{ext}} = \mathbf{0} \tag{3}$$

$$\mathbf{G} = \mathbf{Y} \cdot \mathbf{A^T} \cdot \mathbf{P} + \mathbf{Y} \cdot \boldsymbol{\tau} \tag{4}$$

The unknown terms in Eq. (3) and Eq. (4) are: array **G** (length: *NB*), containing the mass flow rates in each branch, array **P** (length: *NN*), composed by the values of pressure at each node. The known terms are: the aforementioned incidence matrix **A** (size: *NN* × *NB*); array $\mathbf{G_{ext}}$ (length: *NN*), which contains the mass flow rates injected in or extracted from the system; fluid dynamic conductance matrix **Y** (size: *NB* × *NB*), accounting for the pressure losses; vector $\boldsymbol{\tau}$ (length: *NB*), which represents the pressure rise due to pumps. A detailed description of the algorithm used for the solution of the hydraulic problem can be found in Sciacovelli et al. [22].

2.2 The thermal problem

In order to predict the thermal behavior of the network, the energy conservation equation must be solved for the whole system. In this paper, four different formulations have been used for the thermal problem. All of them rely on some common assumptions:

- the fluid is incompressible;
- the specific heat is constant;
- the axial thermal conduction is ignored;
- the ground heat capacity is neglected.

First, the following three models were analyzed:

a) **(*One-equation model*, Approach a)** The first formulation is based on a single Partial Differential Equation – Eq. (5), which describes the thermal evolution of the water flowing in the pipe. The heat capacities of the steel pipe and of the insulation layer are neglected. As represented in Figure 1(a), just the fluid heat capacity is considered.

$$\rho_w c_{p,w} \frac{\partial T_w}{\partial t} + \rho_w c_{p,w} v_w \frac{\partial T_w}{\partial x} + \varphi_{loss,w \to g} = 0 \tag{5}$$

The first term in Eq. (5) represents the transient term, which contains the water density ρ_w, the specific heat capacity of water $c_{p,w}$ and the water temperature T_w partial derivative with respect to time t. The second term is the convective term, in which v_w represents the water velocity and x the spatial coordinate. Finally, $\varphi_{loss,w \to g}$ accounts from the thermal losses from water to ground.

b) **(*Two-equations model*, Approach b)** The second formulation involves two coupled PDEs to include the thermal evolution of water and steel. The equations are reported in Eq. (6). This formulation takes into account the heat capacities of water and steel pipe, while the insulation heat capacity is neglected. A schematic representation is given in Fig. 1(b).

$$\begin{cases} \rho_w c_{p,w} \frac{\partial T_w}{\partial t} + \rho_w c_{p,w} v_w \frac{\partial T_w}{\partial x} + \varphi_{loss,w\to s} = 0 \\ \\ \rho_s c_{p,s} \frac{\partial T_s}{\partial t} + \varphi_{loss,s\to w} + \varphi_{loss,s\to g} = 0 \end{cases} \tag{6}$$

In this case, the first equation reported in Eq. (6) represents the thermal evolution of water and differs from Eq. (5) in that the thermal losses taken into account ($\varphi_{loss,w\to s}$) are from water to steel. The second equation represents the thermal evolution of steel temperature T_s. ρ_s and $c_{p,s}$ respectively represent the steel density and specific heat. As for the thermal sources/losses, both the contributions towards water $\varphi_{loss,s\to w}$ and ground $\varphi_{loss,s\to g}$ must be taken into account.

c) **(*Three-equations model*, Approach c)** A third formulation is used to include the heat capacity of the insulation, as illustrated in Fig. 1(c). Three coupled PDEs – reported in Eq. (7) – are used to describe the thermal transient of water, steel and of the insulation layer. This is the most accurate approach among the ones proposed in this paper. On the other hand, the problem could become computationally intensive.

$$\begin{cases} \rho_w c_{p,w} \frac{\partial T_w}{\partial t} + \rho_w c_{p,w} v_w \frac{\partial T_w}{\partial x} + \varphi_{loss,w\to s} = 0 \\ \\ \rho_s c_{p,s} \frac{\partial T_s}{\partial t} + \varphi_{loss,s\to w} + \varphi_{loss,s\to ins} = 0 \\ \\ \rho_{ins} c_{p,ins} \frac{\partial T_{ins}}{\partial t} + \varphi_{loss,ins\to s} + \varphi_{loss,ins\to g} = 0 \end{cases} \tag{7}$$

The expression for the water thermal evolution is the first one reported in Eq. (7) and it is the same as in the previous case. Instead, the second equation, which describes the steel temperature evolution, differs from the one of Approach (c) due to the thermal losses, which in this case are computed from steel to insulation ($\varphi_{loss,s\to ins}$). The last equation is the insulation equation. The first term is again the transient term, which includes the insulation density ρ_{ins}, its specific heat $c_{p,ins}$ and the insulation temperature T_{ins} temporal derivative. The sources/losses include both the contributions to the steel pipe $\varphi_{loss,ins\to s}$ and the ground $\varphi_{loss,ins\to g}$.

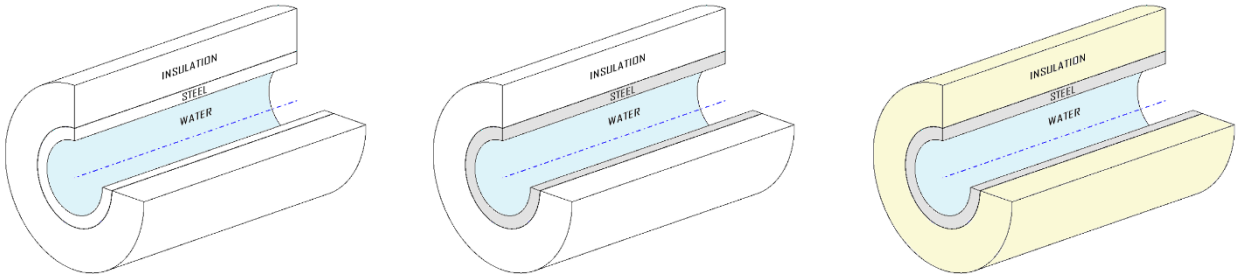

(a) (b) (c)

FIGURE 1. Graphical representation of a portion of the pipe. Colored parts are associated to heat capacities which are included in each model. In detail, model (a) just takes into account the water heat capacity; in model (b) the heat capacities of water and steel are considered; finally, model (c) involves the consideration of the heat capacities of water, steel and insulation.

In order to solve the thermal problem, the different equations were integrated over their corresponding control volumes. As previously mentioned, the number of control volumes used for the solution of the energy conservation equations is greater than that used for the hydraulic problem ($NN' > NN$ and $NB' > NB$). This aims at reducing the effect of artificial diffusivity and increases the accuracy of the solution. The Upwind Differencing Scheme [20] was used to relate boundary and nodal values of temperature.

Then, the matrix form of the problem – given in Eq. (8) – was obtained.

$$\mathbf{M} \cdot \dot{\mathbf{T}} + \mathbf{K} \cdot \mathbf{T} = \mathbf{g} \tag{8}$$

The size and the meaning of the terms in Eq. (8) are different according to the model formulation adopted. They are summarized in Table 1. While in case (a) the unknown vector accounts for the nodal values of water temperature, in case (b) and (c) it also takes into account respectively the nodal temperature values of steel and of steel and insulation.

TABLE 1. Description and size of the arrays and matrices in the energy conservation equation – Eq. (8).

Term	Description	Size		
		Approach (a)	Approach (b)	Approach (c)
T	Unknown vector	$NN' \times 1$	$2NN' \times 1$	$3NN' \times 1$
M	Mass matrix	$NN' \times NN'$	$2NN' \times 2NN'$	$3NN' \times 3NN'$
K	Stiffness matrix	$NN' \times NN'$	$2NN' \times 2NN'$	$3NN' \times 3NN'$
g	Known terms vector	$NN' \times 1$	$2NN' \times 1$	$3NN' \times 1$

2.3 Equivalent thermal model

In this paper a further approach is presented to achieve a trade-off between time and accuracy; this is an equivalent one-equation model. It takes into account the heat capacities of water and steel in a unique equation, thanks to the assumption that the pipe immediately reaches the thermal equilibrium with the water. As a consequence, the steel temperature is assumed equal to the water temperature, and the thermal resistance between the two is considered equal to zero. This is a reasonable assumption, since the heat transfer between water and steel is very high.

This model (***Equivalent one-equation model*, Approach d)** relies on the Partial Differential Equation reported in Eq. (9). With respect to Eq. (5), this equation considers a greater thermal inertia for the fluid.

$$(\rho_w c_{p,w} + \rho_s c_{p,s}) \frac{\partial T_w}{\partial t} + \rho_w c_{p,w} v_w \frac{\partial T_w}{\partial x} + \varphi_{loss,s\to g} = 0 \tag{9}$$

The first term reported in Eq. (9) represents the transient term and includes both the heat capacities of water and steel. Once integrated over the i-th control volume, this term becomes

$$(\rho_w c_{p,w} V_w^i + \rho_s c_{p,s} V_s^i) \frac{\partial T_w}{\partial t}$$

where V_w^i and V_s^i are respectively the water volume and the steel volume. The second term in Eq. (9) is the convective term. Finally, the last term accounts for the thermal dispersion to the ground.

As for the matrix form of the problem, the meaning and the size of the arrays and matrices is the same as in the Approach (a) (see Table 1). Only the matrix **M** is slightly different since in this last case it contains both water and steel thermal inertia.

Overall, thanks to this approximation, the steel heat capacity can be included in the model without weighing down the simulation. To evaluate the performances of this approach, an application to the pure advection problem previously stated is performed.

3. Application

In this paper, four different approaches to the numerical solution of the thermal problem were proposed: a one-equation model which just solves the energy conservation equation for the fluid; a two-equations model involving the

energy conservation equations for the fluid and the steel pipe; a three-equations model which considers the fluid, the steel pipe and the insulation layer; finally, an equivalent one-equation model which combines the fluid and the steel pipe, considering both the heat capacities in a unique equation.

At first, the four models proposed and described in Section 2 were tested on a pure advection problem over a pipe. The test involved a constant water mass-flow rate flowing in a pipe which had a length of 1 km and internal diameter, external diameter and insulation thickness respectively equal to 50 mm, 125 mm and 29 mm. The water in the pipe was supposed at an initial temperature of 15 °C. Then, a mass-flow rate at 120 °C was injected at the inlet section. This is to simulate a start-up transient after the night set-back. The water velocity was imposed equal to 0.3 m/s. The ground temperature was supposed to be 15 °C. A thermal transient was simulated using the three thermal models. All the simulations were conducted with very fine spatial and temporal discretization ($\Delta x = 0.01\ m$ and $\Delta t = 0.1\ s$) in order to minimize the numerical error.

Then, the two one-equation models – Approach (a) and Approach (d), which according to the first tests resulted to be the most performing ones – were used to perform a comparison in the case of a real system. The case-study analyzed belongs to the Turin district heating network, which is the largest in Italy and one of the largest in Europe. It satisfies the thermal request of more than 5000 buildings, which have a total volume of about 56 million m^3.

The network can be imagined as composed of two interconnected parts: the transport network and the distribution network. The transport network is the backbone of the system and is composed by pipes with larger diameters. It connects the thermal plants to the various areas of the city. The distribution network, instead, connects the transport network to the buildings located in an area. Connection points between the distribution networks and the transport network are called the thermal barycenters.

In the Turin district heating network, six thermal plants are available. Among them, there are three cogeneration units, which can produce up to 760 MW of heat. Then, the production capacity is completed by means of heat-only boilers and thermal storages. The supply temperature is kept close to the nominal one, that is about 120 °C in winter and over 90 °C in summer; the temperature on the return pipeline depends on the thermal load.

For this analysis, a simulation of the thermo-fluid dynamic behavior of a distribution network during a typical winter day was carried out. The selected distribution network connects 66 buildings to the main pipeline. A schematic of the network is reported in Figure 2. The mass-flow rates extracted by each building and the expected thermal profiles were obtained from the data gathering system, which is installed in building's substations for billing purposes.

The simulation was performed for both the supply and return lines of the network. The time-step adopted for the solution of the thermal problem was equal to $10\ s$. For what concerns the spatial discretization, nodes were placed with a granularity of 1 node per meter.

The two one-equation models were used to evaluate the temperature of the water coming back at the barycenter through the return line ($T_{return,BCT}$). Also, the heat flux request of the distribution network at the barycenter level was evaluated by means of the formula reported in Eq. (10):

$$\Phi_{tot,BCT}(t) = G_{tot,BCT}(t) c_p (T_{supply,BCT} - T_{return,BCT}(t)) \tag{10}$$

where $G_{tot,BCT}$ represents the total mass flow rate and $T_{supply,BCT}$ is the supply temperature of the distribution network (equal to 118 °C in this case).

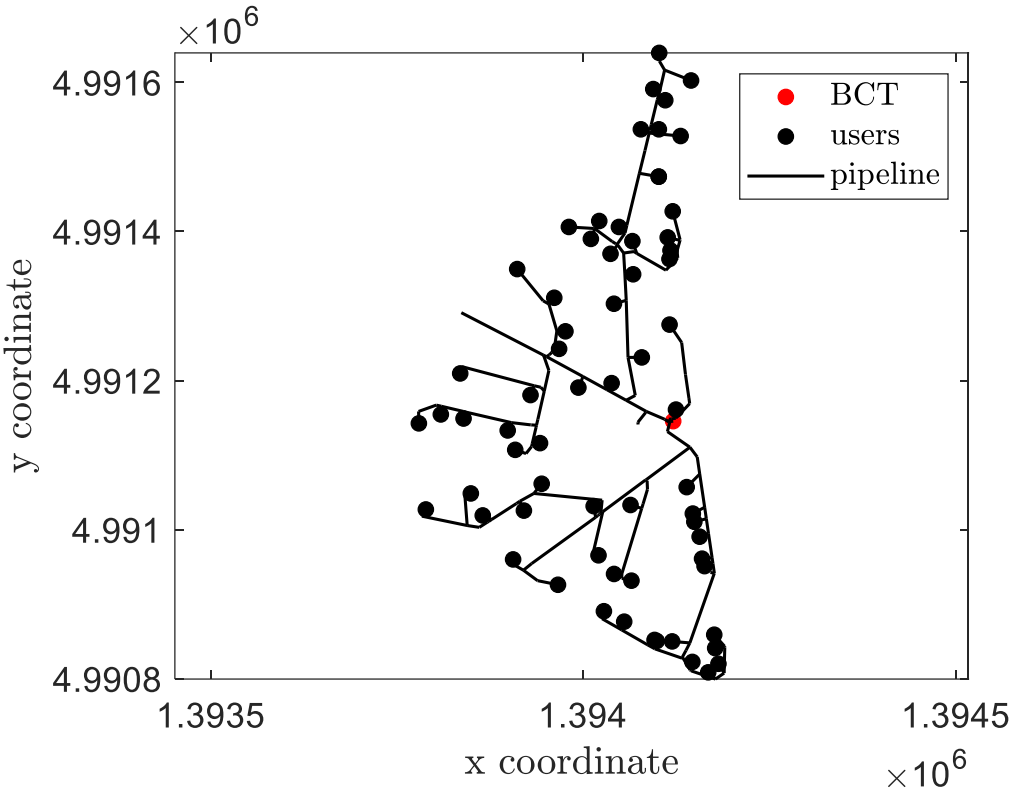

FIGURE 2. Graphical representation of the distribution network.

4. Results and discussion

The goal of this paper was to provide a quantitative analysis of the influence of the heat capacities of the steel pipe and of the insulation layer on the thermal response in district heating systems, in order to get a better view of the approximations introduced in numerical thermal models. To do that, four different approaches have been taken under consideration. The four approaches have been compared first on a transient pure advection problem over a pipe (results reported in section 4.1), and then in a real case-study (results reported in section 4.2).

4.1 Transient pure advection problem

A pure advection transient problem over a single pipe was simulated to compare the different approaches proposed in this paper. A detailed description of the test parameters is reported in Section 3.

Figure 3 shows the results provided by the various approaches in terms of spatial temperature distribution. In Figure 3(a), the water temperature distribution over the pipe after 40 minutes – obtained using Approach (a) – is illustrated. Approach (b) allows to obtain the temperature distribution of both water and steel, as reported in Figure 3(b). The three-equations model expressed by Approach (c) solves the energy equation of water, steel and insulation; their temperature distributions are depicted in Figure 3(c). The solution of Approach (c) represents the most accurate among the ones proposed in this paper. Since the relative error between the water temperature distribution and the steel temperature distribution is only 1.4% at $t = 40\ min$, these two temperatures could be considered as equal with negligible loss of accuracy. Hence, the approximation introduced by the equivalent thermal model – Approach (d) – can be considered as acceptable. Vice versa, it is not possible to introduce the same approximation for the insulation layer since its temperature profile is quite different. Finally, Figure 3(d) displays the solution produced by Approach (d), which just involves water temperature.

The differences among the water temperature profile provided by each model are highlighted in Figure 4. It is worth to observe that the *hydraulic front* – which represents, at each time step, the coordinate of the extreme point reached by the mass-flow rate and can be computed as $x(t) = x_0 + v \cdot (\mathrm{t} - \mathrm{t}_0)$ – is located at $x = 720\ m$ after 40 minutes. By comparing the temperature distributions obtained with the one-equation model (*1 PDE*) and with the two-equations model (*2 PDEs*), it comes out that the consideration of the steel pipe heat capacity significantly modifies the solution of the problem, since it is responsible for the cool-down of a relevant portion of the mass-flow rate. On the other hand, introducing a further partial differential equation (*3 PDEs*) to take into account the transient in the insulation layer does not produce relevant additional improvements (relative error equal to 0.1 %). Finally, the equivalent one-equation model (labelled as *1 eq. PDE*) is capable to capture the thermal delay due to the steel pipe heat capacity, despite it does not reproduce the smoothing of the solution.

In Figure 5, the water temperature evolution of the control volume located at $x = 500\ m$ is reported. While in the one-equation model – Approach (a) – the temperature of the control volume considered steeply rises to 120 °C at $t = 27.8\ min$, in the solutions obtained with the two most precise models – Approach (b), i.e. the two-equations model, and Approach (c), i.e. the three-equations model – this temperature change is delayed and gradual. Particularly, the temperature gradually increases from 15 °C to 120 °C in the time range between 35 and 60 minutes. The equivalent one-equation model – Approach (d) – is able to take into account the time delay due to the greater thermal inertia and shifts the temperature change at $t = 47.2\ min$, with a 19.4 minutes delay with respect to Approach (a). Again, it can be observed that, in this case, the temperature change is sharp.

Since the temperature rise in the equivalent thermal model is abrupt, the concept of *equivalent thermal front* can be introduced. The equivalent thermal front can be defined as the coordinate of the extreme "hot" point of the mass-flow rate and can be computed as $x(t) = x_0 + v_{th,eq} \cdot (\mathrm{t} - \mathrm{t}_0)$, where $v_{th,eq}$ is the *equivalent thermal velocity*, i.e. the propagation speed of the thermal perturbation. The equivalent thermal velocity can be expressed as:

$$v_{th,eq} = v_w \frac{\rho_w c_{pw} V_w}{\rho_w c_{pw} V_w + \rho_s c_{ps} V_s} \tag{11}$$

In the specific case, the equivalent thermal velocity assumes the value of about 0.18 m/s, with a hydraulic velocity of 0.3 m/s. Generally, it depends on the steel mass of the pipe and, in particular, it decreases as the ratio between the volumes of steel and water increases. As a consequence, the larger the volume ratio, the larger the delay.

The hydraulic front and the equivalent thermal front are represented in Figure 6, where the water temperature along the pipe is reported at $t = 40\ min$. While in the solution provided by the one-equation model (a), the hydraulic front is coincident with the thermal front, the two-equations (b) and the three-equations models (c), which are the ones that represent in the most appropriate way the real physical problem, the thermal drop occurs in a *thermal drop region*, which is delayed with respect to the hydraulic front. Finally, in the equivalent one-equation model (d) it is possible to recognize the equivalent thermal front, which is capable to take into account the delay although the temperature gap is sharp.

The computational time required by each approach for the solution of the 40-minutes thermal transient is reported in Table 2. For the one-equation approach (a), the simulation lasts approximately 1 minute. Instead, the two-equations (b) and the three-equations models (c) require respectively about 26 minutes and 4.2 hours. Finally, the same simulation can be performed in less than 1 minute using the equivalent one-equation model (d). The solution of the problem shown in Figure 4 and Figure 5 and the analysis of these data clearly suggest that the best trade-off between performance and accuracy is provided by the equivalent one-equation model, Approach (d). On the other hand, the use of model (a) is not highly recommended, since the computational time is of the same order of magnitude, but it is less accurate. Then, despite the two-equations model (b) is more precise with respect to the equivalent approach (d), it is unusable for application to real case studies due to its high time complexity. Finally, it is quite evident that the computational time required by Approach (c) makes it inapplicable even for applications to small test-cases. Indeed, this approach introduces an unjustified increase in computational cost, given that, as previously stated, the quality of the solution does not significantly improve with respect to Approach (b). Hence, this study suggests that is to advisable to use the equivalent thermal model – Approach (d), which allows a reduction in the computational time of 96.4 % and 99.6 % with respect to – respectively – Approaches (b) and (c), at the costs of a reduction in accuracy in the reproduction of the smoothness of the solution. However, it may be observed that this kind of error could – generally speaking – counteract the truncation error introduced by artificial diffusivity (numerical diffusivity), which tents to smooth the solution.

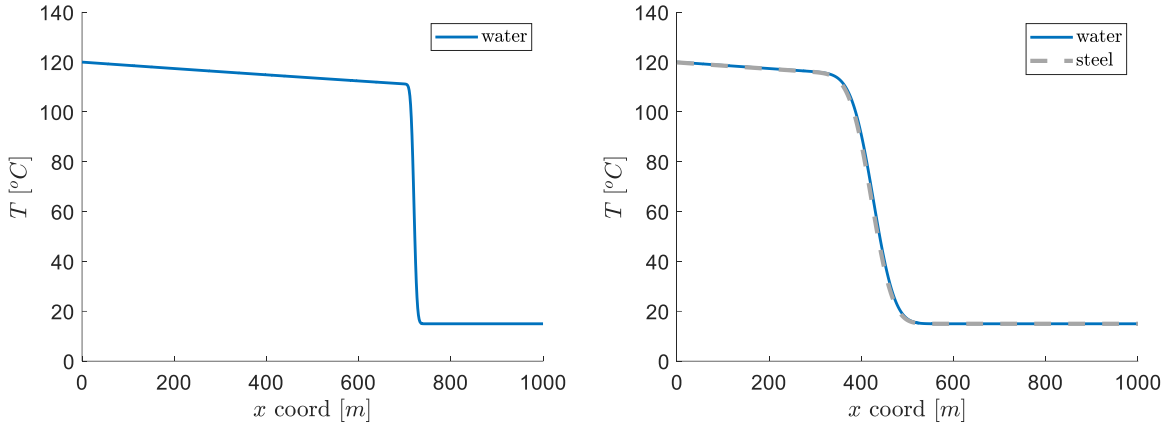

(a) One-equation thermal model

(b) Two-equations thermal model

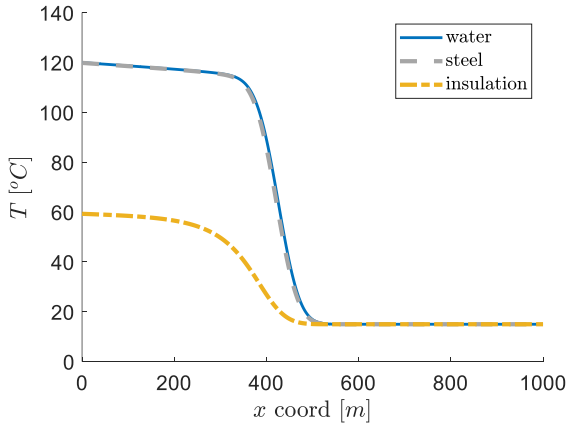

(c) Three-equations thermal model

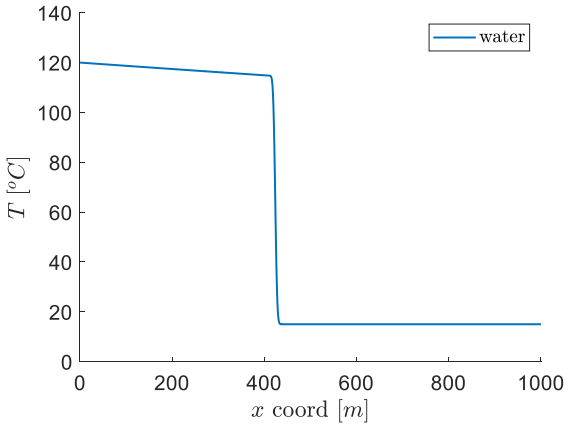

(d) One-equation equivalent thermal model

FIGURE 3. Temperature distributions obtained with the four approaches (Approaches (a) to (d)) for a transient pure advection problem in a pipe (length = 1 km, internal diameter = 50 mm, external diameter = 125 mm, insulation thickness = 29 mm, fluid velocity = 0.3 m/s, initial temperature = 15 °C, ground temperature = 15 °C, inlet temperature = 120 °C) after 40 minutes.

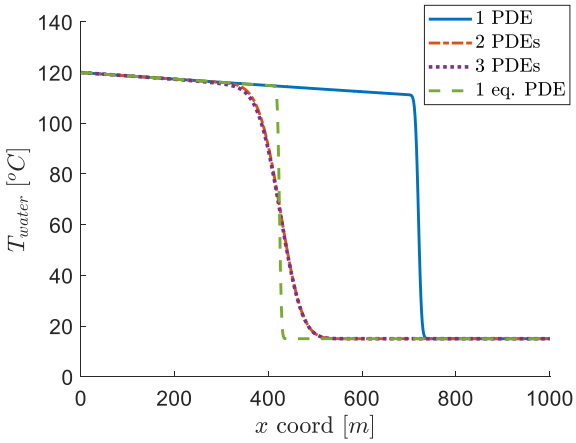

FIGURE 4. Water temperature distribution obtained with the four approaches (Approaches (a) to (d)) for a transient pure advection problem in a pipe (length = 1 km, internal diameter = 50 mm, external diameter = 125 mm, insulation thickness = 29 mm, fluid velocity = 0.3 m/s, initial temperature = 15 °C, ground temperature = 15 °C, inlet temperature = 120 °C) after 40 minutes. The hydraulic front is located at x = 720 m.

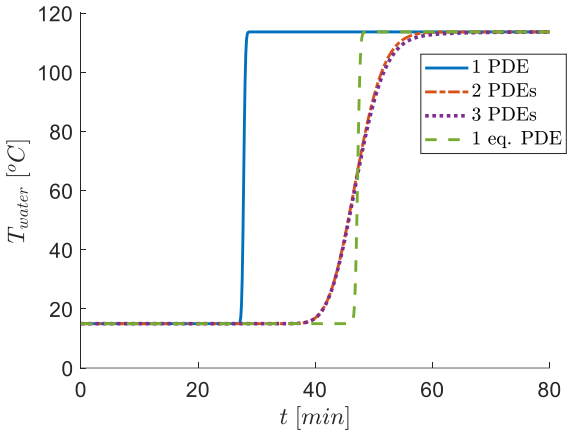

FIGURE 5. Water temperature evolution for a pure advection problem in a pipe (length = 1 km, internal diameter = 50 mm, external diameter = 125 mm, insulation thickness = 29 mm, fluid velocity = 0.3 m/s, initial temperature = 20 °C, inlet temperature = 120 °C) at x = 500 m using the four models (Approaches (a) to (d)).

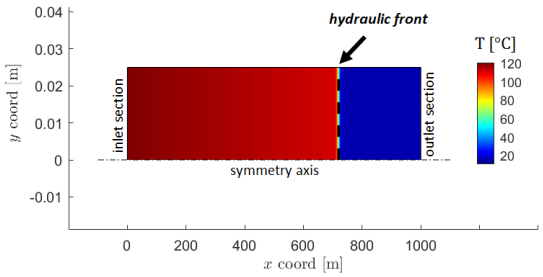

(a) One-equation thermal model

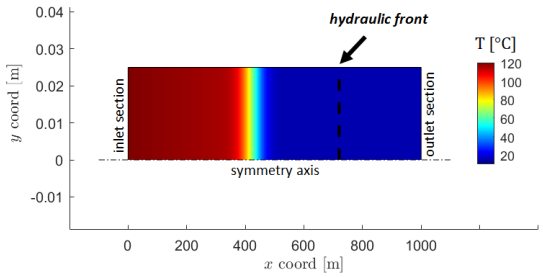

(b) Two-equations thermal model

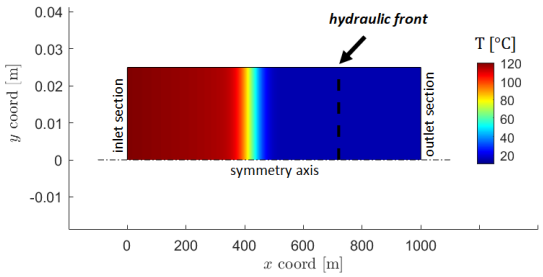

(c) Three-equations thermal model

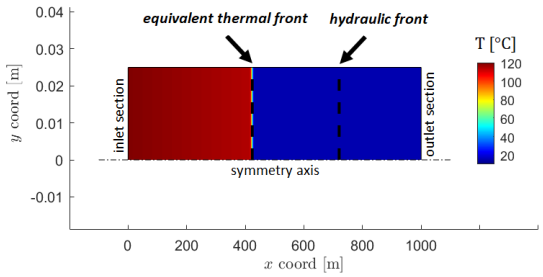

(d) One-equation equivalent thermal model

FIGURE 6. Water temperature along the pipe at t = 40 min for a pure advection problem (length = 1 km, internal diameter = 50 mm, external diameter = 125 mm, insulation thickness = 29 mm, fluid velocity = 0.3 m/s, initial temperature = 15 °C, ground temperature = 15 °C, inlet temperature = 120 °C).

TABLE 2. Computational time required for the solution of a 40-minutes-lasting transient pure advection problem in a pipe 1 km long, with dx = 0.01 m and dt = 0.1 s, using the four approaches presented in this paper. All simulations were run on a PC laptop with a total of 16 GB of memory and an Intel i7-8565U CPU @ 1.80 GHz. The software MATLAB® was used and the function adopted for the solution of the linear systems was *mldivide* with its default options.

Approach	Number of PDEs	Water heat capacity	Pipe heat capacity	Insulation heat capacity	Equivalent approach	Computational time [s]
(a)	1	✓				61
(b)	2	✓	✓			1544
(c)	3	✓	✓	✓		15098
(d)	1	✓	✓		✓	55

4.2 Real case-study

In this section, results of the application to the distribution network belonging to the Turin district heating network are reported. The simulation has been carried out for a typical winter day with the standard one-equation model (Approach a) and the equivalent one-equation model (Approach d). The temperature evolution of the mass-flow rate in the return line at the barycenter level (which is the connection point of the distribution network with the transport network) is reported in Figure 7(a). The thermal delay due to the increased heat capacity is particularly evident in the early morning, during the heating phase of the system. The relative error is around 3.8% and the maximum temperature difference among the curves obtained with the two approaches is of 8 °C. The thermal load of the whole distribution network is illustrated in Figure 7(b). In this case, the differences between the two approaches are less relevant; the relative error is 2.1 %. However, it is worth to observe that the modification of the thermal response of the network may cause important implications in some applications, like for example optimization applications.
Finally, the results obtained with the one-equation equivalent model are compared to real measurements for validation purposes. Figure 8(a) shows the comparison among the measured and computed *switch-on time* of each user (which is represented by the time that is needed by the temperature perturbation to reach each user's substation). The experimental data were obtained from the gathering system of the substations that has a discretization of 5 minutes. It is possible to appreciate that the great majority of the computed results are within a 15-minutes tolerance with respect to the measured data. In Figure 8(b), the water temperature evolution at the inlet of a user's substation is reported; in this case, the model gives a result that is approximately 6 minutes in advance with respect to the measurements. If one considers that the experimental measures are also subject to uncertainty, the computational result turns out to be an excellent reproduction of the physical phenomenon.

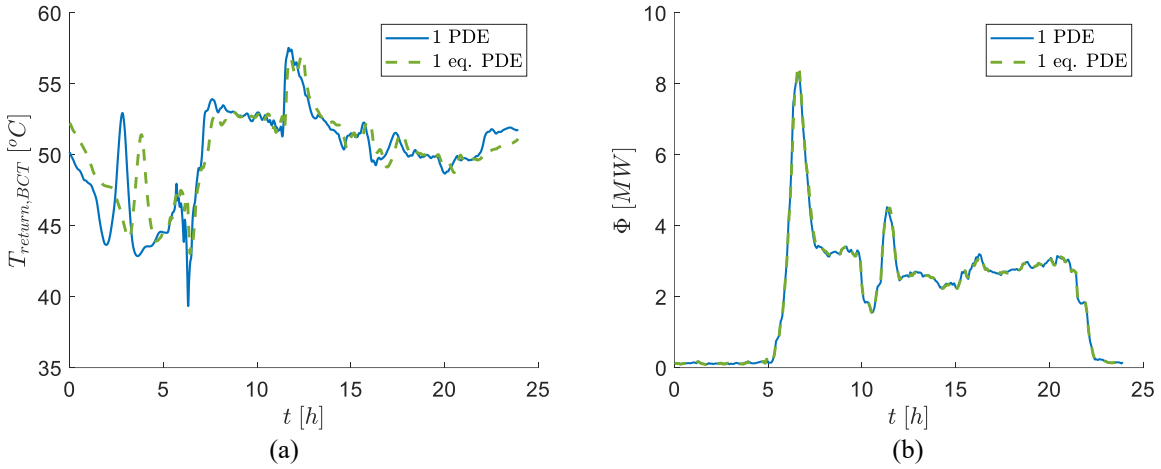

FIGURE 7. Temperature of the mass-flow rate coming back to the barycenter (a) and thermal load of the distribution network (b) depicted in Figure 2, obtained with the simulation of a 24-hours thermal transient for a typical winter day. The blue line represents the solution obtained with the standard one-equation model; the green dashed line represents the solution obtained with the equivalent one-equation model.

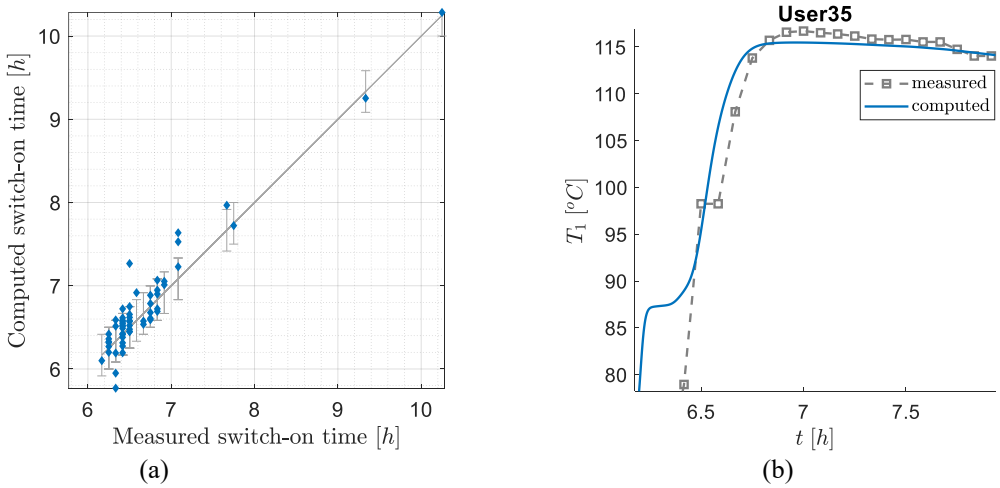

FIGURE 8. Comparison of the measured and computed switch-on time of each user of the network (a); details of the temperature evolution at user 35 (b).

5. Conclusions

The present work was aimed at assessing the impact of the pipeline thermal capacity in district heating network modelling and proposing a proper approach to simulate the thermal transients precisely and with reasonable computational costs.

These goals were reached by comparing four different approaches. The first is based on a single partial differential equation, which describes the thermal evolution of water and neglects the influence of the heat capacities of the steel and of the insulation, in the wake of what has been done by various authors in literature [12-13,19]. The second one uses two partial differential equations to represent the transients in both water and steel, while the heat capacity of the insulation is again neglected, as done by [10,15-17]. The third approach involves all the three contributions and is made up by three partial differential equations. Finally, a fourth formulation is proposed as an innovative solution that

combines the heat capacity of steel and water in an equivalent one-equation model, which is based on the assumption of equal temperatures in the two bodies.

The approaches were firstly tested on a transient pure advection problem on a pipe and secondly the standard one-equation model and the equivalent one-equation model were compared on a real case-study, taken from the Turin district heating network.

The main results of the analysis are the following:

- the steel heat capacity has a significant influence on the thermal response of the system, being responsible for a time delay in temperature propagation; instead, the insulation heat capacity does not make the solution much different. Hence, it is worth to include the steel heat capacity in the model, while the insulation heat capacity can be neglected without loss of accuracy.
- the equivalent one-equation model, including water and steel heat capacities in a single partial differential equation, appears to be the best choice among the proposed approaches. The approximation introduced is affordable and the temperature delay is reproduced in a sufficiently accurate way. Moreover, the use of the equivalent one-equation model substantially reduces the computational time required for the simulation (over than 96% computation time reduction), making this approach the best trade-off between performance and accuracy.

Acknowledgments

Authors acknowledge the IREN company for providing the data used in this work.

Nomenclature

c_p	Specific heat [J/kg/K]
p	Pressure [Pa]
t	Time [s]
T	Temperature [K]
v	Velocity [m/s]
V	Volume [m^3]
x	Position [m]

Greek symbols

ρ	Density [kg/m^3]
φ_{loss}	Volumetric heat losses [W/ m^3]
Φ_{tot}	Total thermal load [W]

Abbreviations and subscripts

BCT	Barycenter
g	Ground
ins	Insulation
NB	Number of branches
NN	Number of nodes
s	Steel
w	Water

References

1. T. Laajalehto, M. Kuosa, T. Mäkilä, M. Lampinen, R. Lahdelma, *Energy efficiency improvements utilizing mass flow control and a ring topology in a district heating network*, Applied Thermal Engineering 69, 86-95 (2014).
2. D. Connolly, H. Lund, B.V. Mathiesen, S. Werner, B. Möller, U. Persson, T. Boermans, D. Trier, P.A. Østergaard, S. Nielsen, *Heat Roadmap Europe: Combining district heating with heat savings to decarbonize the EU energy system*, Energy Policy 65, 475-489 (2014).
3. P. Woords and J. Overgaard, "Historical development of district heating and characteristics of a modern district heating system", in *Advanced District Heating and Cooling (DHC) Systems*, edited by R.Wiltshire (Woodhead Publishing Series in Energy, 2016), pp. 3-15.
4. N. Nord, E. K. L. Nielsen, H. Kauko, T. Tereshchenko, *Challenges and potentials for low-temperature district heating implementation in Norway*, Energy 151, 889-902 (2018).

5. H. Lund, S. Werner, R. Wiltshire, S. Svendsen, J.E. Thorsen, F. Hvelplund, B.V. Mathiesen, *4th Generation District Heating (4GDH) Integrating smart thermal grids into future sustainable energy systems,* Energy 68, 1-11 (2014).
6. H. Lund, P.A. Østergaard, M. Chang, S. Werner, S. Svendsen, P. Sorknæs, J.E. Thorsen, F. Hvelplund, B.O.G. Mortensen, B.V. Mathiesen, C. Bojesen, N. Duic, X. Zhang, B. Möller, *The status of 4th generation district heating: Research and results*, Energy 164, 147-159 (2018).
7. H. Pálsson, H. Larsen, H. Ravn, B. Bohm, J. Zhoud, *Equivalent Models of District Heating Systems*, Proceedings of the 7th International Symposium on District Heating and Cooling (1999).
8. M. Betancourt Schwartz, M. T. Mabrouk, C. Santo Silva, P. Haurant, B. Lacarrière, *Modified finite volumes method for the simulation of dynamic district heating networks*, Energy 182, 954-964 (2019).
9. A. Benonysson, *Dynamic modelling and operational optimization of district heating systems*, Laboratory of Heating and Air Conditioning, Technical University of Denmark (1991).
10. I. Gabrielaitiene, B. Bøhm, B. Sunden, *Evaluation of Approaches for Modeling Temperature Wave Propagation in District Heating Pipelines*, Heat Transfer Engineering 29, 45-56 (2008).
11. V.D. Stevanovic, B. Zivkovic, S. Prica, B. Maslovaric, V. Karamarkovic, V. Trkulja, *Prediction of thermal transients in district heating systems*, Energy Conversion and Management 50, 2167-2173 (2009).
12. Y. Wang, S. You, H. Zhang, X. Zheng, W. Zheng, Q. Miao, G. Lu, *Thermal transient prediction of district heating pipeline: Optimal selection of the time and spatial steps for fast and accurate calculation*, Applied Energy 206, 900-910 (2017).
13. L. Vasek, V. Dolinay, V. Vasek, *Pulled Plug-flow Model for 4th Generation District Heating*, IFAC PapersOnLine 52-4, 12-17 (2019).
14. G. Barone, A. Buonomano, C. Forzano, A. Palombo, *A novel dynamic simulation model for the thermo-economic analysis and optimisation of district heating systems*, Energy Conversion and Management 220, 113052 (2020).
15. J. Zheng, Z. Zhou, J. Wang, *Function method for dynamic temperature simulation of district heating network*, Applied Thermal Engineering 126, 682-688 (2017).
16. P. Jie, Z. Tian, S. Yuan, N. Zhu, *Modeling the dynamic characteristics of a district heating network*, Energy 39, 126-134 (2012).
17. H. Wang & H. Meng, *Improved thermal transient modeling with new 3-order numerical solution for a district heating network with consideration of the pipe wall's thermal inertia*, Energy 160, 171-183 (2018).
18. K. Sartor & P. Dewalef, *Experimental validation of heat transport modelling in district heating networks*, Energy 137, 961-968 (2017).
19. J. Vivian, P. Monsalvete Álvarez de Uribarri, U. Eicker, A. Zarrella, *The effect of discretization on the accuracy of two district heating network models based on finite-difference methods*, Energy Procedia 149, 625-634 (2018).
20. F. Harary, *Graph theory*, New Delhi: Narosa Publishing House (1995).
21. H. K. Versteeg, W. Malalasekera, *An introduction to computational fluid dynamics: The finite volume method*, Pearson Education Limited (2017).
22. A. Sciacovelli, V. Verda, B. Borchiellini, *Numerical design of thermal systems*, CLUT Editrice (2015).